Plasmonics (2013) 8:267–275
DOI 10.1007/s11468-012-9384-y

Resonant Mode Analysis of the Nanoscale Surface Plasmon Polariton Waveguide Filter with Rectangle Cavity

Binfeng Yun · Guohua Hu · Yiping Cui

Received: 14 January 2012 / Accepted: 23 May 2012 / Published online: 14 June 2012

Abstract The resonant mode characteristics of the nanoscale surface plasmon polaritons (SPP) waveguide filter with rectangle cavity are studied theoretically. By using the finite difference time domain method, both the band-stop- and band-pass-type rectangle SPP filters are analyzed. The results show that the whispering gallery mode (WGM) and the Fabry–Perot (FP) mode can be supported by the rectangle SPP resonator. Furthermore, both traveling-wave mode and standing-wave mode can be realized by the WGM, while only standing-wave mode can be introduced by the FP mode. The traveling-wave mode can only be realized by the square-shaped SPP resonator, and the traveling-wave mode is splitted into two standing-wave modes by transforming the cavity shape from square to rectangle. Also, the effects of the cavity shape, cavity size, and coupling gap size on the transmission spectra of the SPP resonators are analyzed in detail. This simple SPP waveguide filter is very promising for the high-density SPP waveguide integrations.

Keywords Surface plasmon polariton · Resonator · Rectangle · Filter

Introduction

Surface plasmon polaritons (SPPs) are electromagnetic waves coherently coupled to electron oscillations and propagating at the interface between a dielectric and a metal, with evanescently decaying fields in both sides [1, 2]. With the strong confinement at the dielectric/metal interface, the SPP waveguide can realize subwavelength waveguiding, which is very promising for the high optical integration. There are two basic SPP waveguide configurations, which are the insulator–metal–insulator (IMI) [3, 4] and metal–insulator–metal (MIM) structures [5, 6]. Recently, the MIM SPP waveguide has received plenty of attention because of its nanoscale-waveguiding capability, which cannot be realized by the dielectric waveguide. The SPP waveguide filter is one kind of the important components in the high-density SPP waveguide integration platform. And some kinds of resonance cavity filters based on the MIM SPP waveguides have been proposed, including the circular ring resonators [7–10], rectangle ring resonators [11–13], tooth-shaped resonators [14–17], Fabry–Perot resonators [18–20], nanodisk resonators [21, 22], rectangle cavity resonators [23, 24], and nano-capillary resonators [25]. Among them, the SPP ring resonators and nanodisk resonators have been well-studied, while there are few researches about the rectangle cavity SPP resonators. Comparing to the circular ring SPP resonator, the SPP filter with rectangle cavity is easier for fabrication. But according to the complex geometry than that of the nanodisk SPP resonator, the resonance modes of the rectangle cavity SPP resonator are more geometry-dependent. In Ref. [24], only the first-order resonance mode is used to realize the gain-induced switching. Although the first and second modes are analyzed in Ref. [23], the types of the modes and the mode characteristics of different cavity geometries have not been well-studied. In this article, the resonance mode characteristics of SPP resonator with different rectangle cavity geometries are analyzed in detail. The results show that

Electronic supplementary material The online version of this article (doi:10.1007/s11468-012-9384-y) contains supplementary material, which is available to authorized users.

B. Yun · G. Hu · Y. Cui (✉)
Advanced Photonics Center, Southeast University,
Nanjing, China 210096
e-mail: cyp@seu.edu.cn

Fig. 1 The dependence of Real (n_{eff}) on the fundamental TM mode on the wavelength of incident light λ and the width d

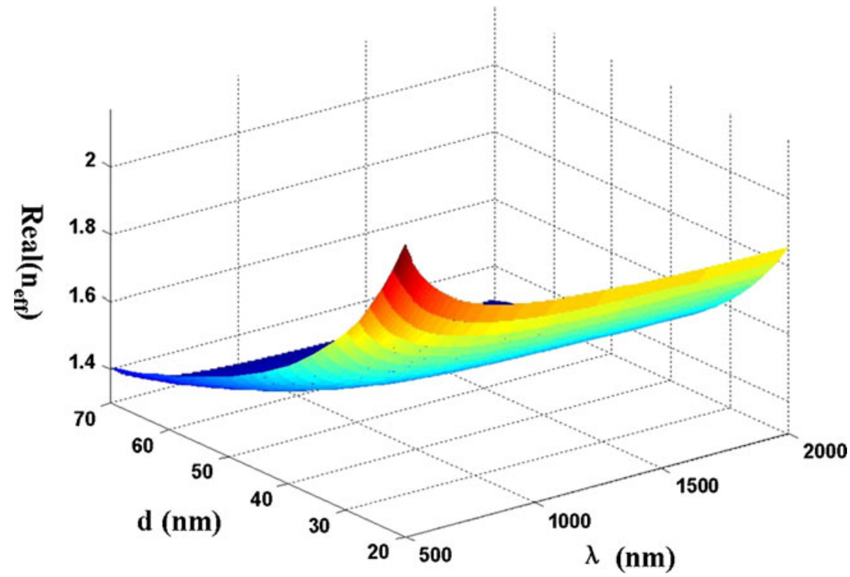

both the whispering gallery mode (WGM) and the Fabry–Perot (FP) mode can be supported by the rectangle SPP resonator. Furthermore, both traveling-wave mode and standing-wave mode can be realized by the WGM, while only standing-wave mode can be introduced by the FP mode. The traveling-wave mode can only be realized with the square-shaped SPP resonator, and the traveling-wave mode is splitted into two standing-wave modes by transforming the cavity shape from square to rectangle. Also, the effects of the cavity shape, cavity size, and coupling gap size on the transmission spectra of the SPP resonators are analyzed in detail.

Dispersion of MIM SPP Waveguide and the FDTD Method

In this article, the MIM SPP waveguide with 50-nm gap size is used as the input/output SPP waveguide, which couples the SPP into a rectangle resonance cavity. With this gap size, only the fundamental transverse magnetic (TM) mode is supported and its dispersion relation is given by:

$$\varepsilon_{\mathrm{in}}k_{z2} + \varepsilon_m k_{z1} \coth\left(-\frac{ik_{z1}}{2}d\right) = 0 \tag{1}$$

Fig. 2 The band-stop filter based on the side-coupled rectangle SPP resonator

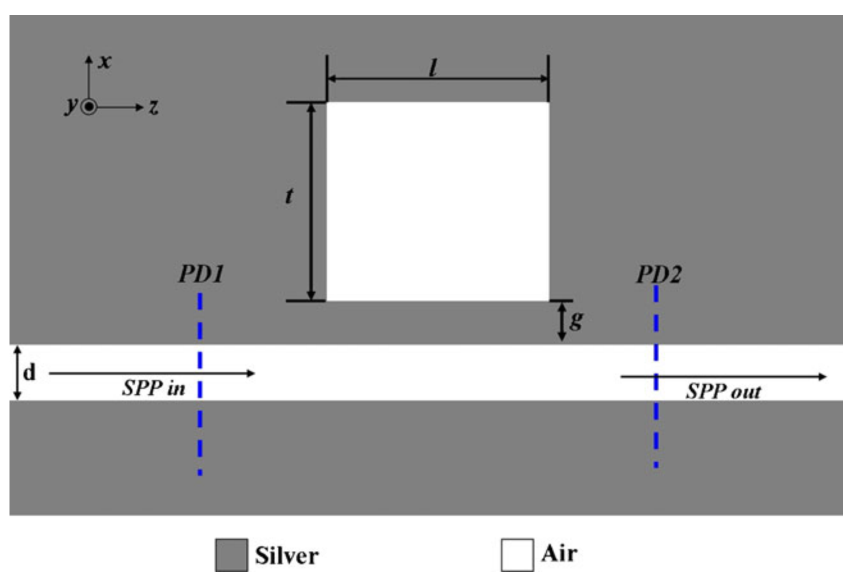

and k_{z1} and k_{z2} are:

$$k_{z1}^2 = \varepsilon_{\text{in}} k_0^2 - \beta^2, k_{z2}^2 = \varepsilon_m k_0^2 - \beta^2 \tag{2}$$

where ε_{in} and ε_m are the dielectric constants of the insulator and the metal, and $k_0=2\pi/\lambda$ is the free-space wave vector. And the dielectric constant of the metal silver is characterized by the Lorentz–Drude model [10, 18]:

$$\varepsilon_m = \varepsilon_\infty - \sum_{m=0}^{5} \frac{G_m \Omega_m^2}{\omega_m^2 - \omega^2 + i\omega\Gamma_m} \tag{3}$$

where ε_∞ is the relative permittivity at the infinity frequency, G_{m} is the oscillator strength, Ω_{m} is the plasma frequency, and ω is the angular frequency of incident light; all these parameters used in the simulations are listed in Ref. [26]. According to Eqs. (1) and (2), the real part of the effective index of the fundamental TM mode ($n_{\text{eff}}=\beta/k_0$) as a function of the slit width w and the incident light wavelength λ is obtained and shown in Fig. 1. The n_{eff} decreases as d increases and decreases relatively slow with an increasing λ.

The 2D FDTD method provided by the Rsoft fullwave package (www.rsoftdesign.com) with perfect matched layer (PML) boundary condition is used to simulate the transmission spectra of the SPP filters. The perfect matched layer is an artificial absorbing material which effectively absorbs field energy that propagates through the PML layers, allowing it to completely leave the domain almost without back reflections. The fundamental TM mode of the MIM waveguide is excited by a dipole source and the mesh grid size is set to 1 nm in order to keep convergence. Two monitors PD1 and PD2 (as shown in Fig. 2) are set to detect the incident power A_1 (without the resonator cavity for reference) and the transmission power A_2 (with the resonator cavity). And the transmittance is defined as $T=A_2/A_1$ [10].

Mode Characteristics of the Band-stop Filter Based on Rectangle SPP Resonator

The structure of the band-stop filter based on the side-coupled rectangle SPP resonator is shown in Fig. 2. The side lengths of the rectangle cavity are l and t, and d and g are the width and the gap size of the MIM waveguide of the coupled region, respectively. The SPP wave is side-coupled into/out the rectangle resonator by the MIM SPP waveguide. The typical transmission spectrum of the band-stop SPP filter with rectangle cavity (l=520 nm, t=500 nm) is shown in Fig. 3. There are five transmission dips according to the resonant modes in the wavelength range of 500~2,000 nm. In order to analysis the effect of the geometry shape of the rectangle resonant cavity, the resonance wavelengths of the first four resonance dips are simulated with a different side length l, while the side length is kept at t=500 nm. The results are shown in Fig. 4. From Fig. 4, it is clear that the resonance wavelength of the first mode is decreased with an increasing l when $l<t$, while the opposite trend is observed when $l>t$. And the second mode has a reversed trend compared to that of the first mode. Also, the resonance wavelengths of the first and second modes intersect at $l=t=$ 500 nm, which means that the first mode and the second mode are degenerated when the shape of the resonance cavity is changed from rectangle to square, while the resonance wavelength of the third mode has a linear relationship with the side length l and increases with increasing l. Also, the fourth mode has the same trend as the first mode.

In order to explain the interesting phenomenon of the different modes, the H_{y} fields of the first four resonant

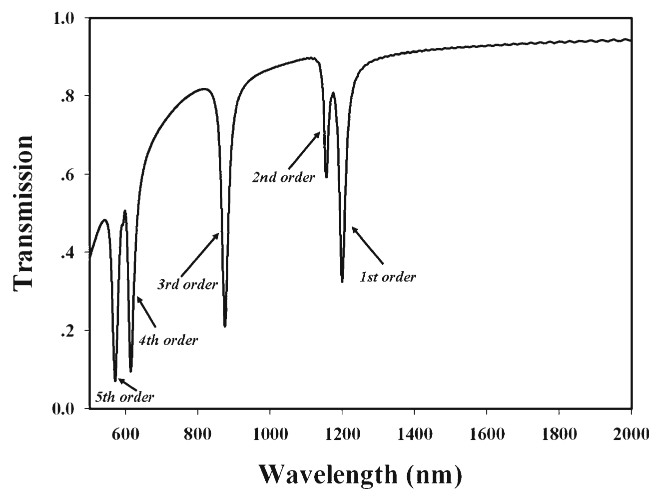

Fig. 3 The transmission spectrum of rectangle cavity (l=520 nm, t=500 nm, g=30 nm)

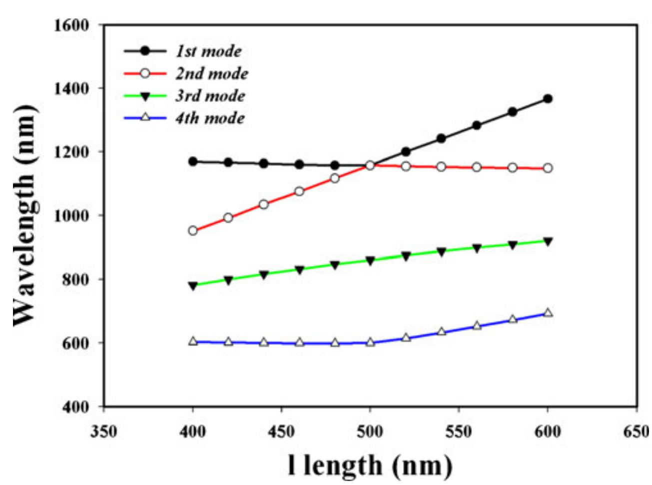

Fig. 4 Resonance wavelengths of rectangle resonator with different l (t=500 nm, g=30 nm)

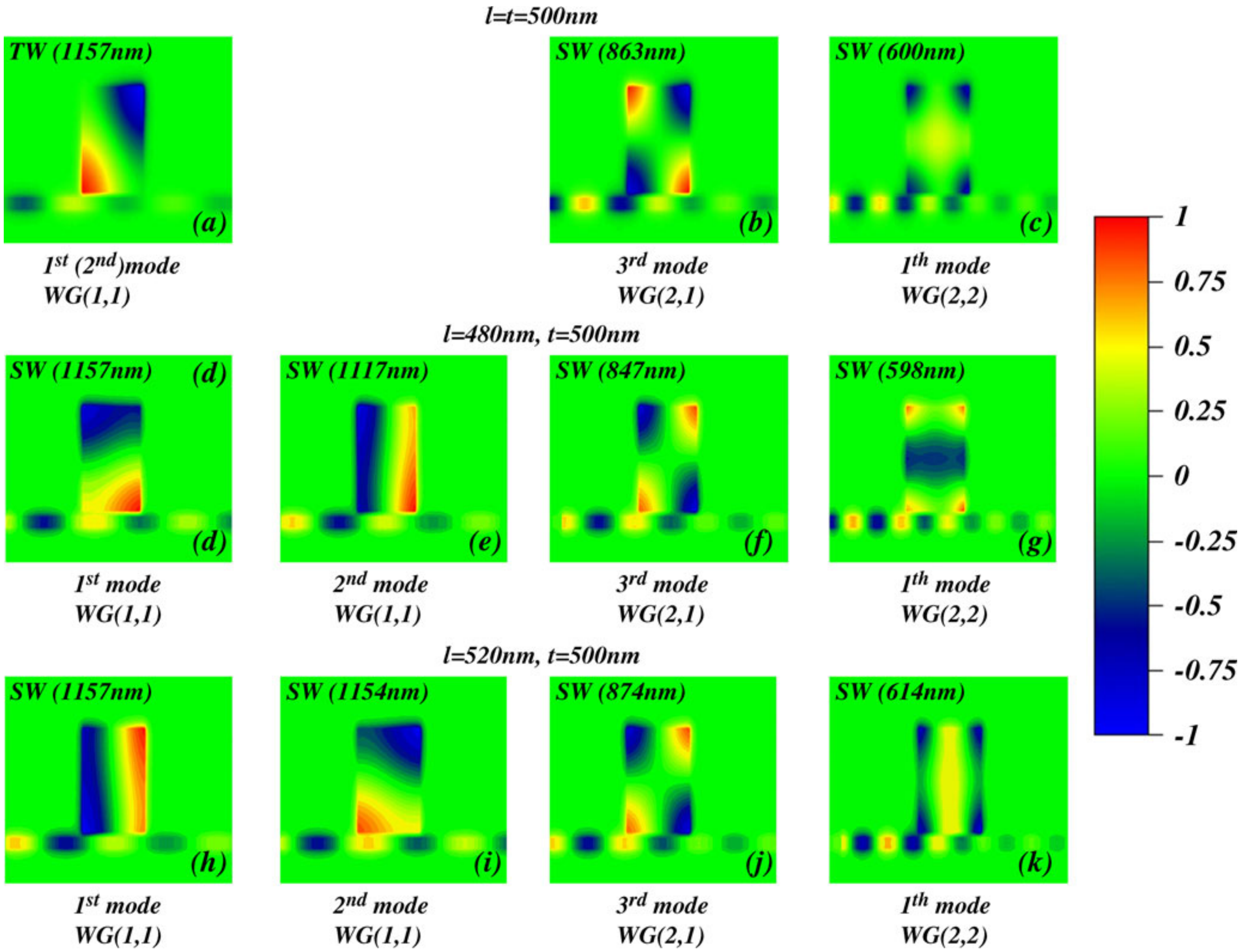

Fig. 5 *a*–*k* The H_y fields of the resonant modes with different geometries

modes are simulated and shown in Fig. 5. The results show that both traveling-wave (TW) and standing-wave (SW) can be realized in the square (l=t) resonant cavity, while only SW can be excited in the rectangle (l≠t) resonant

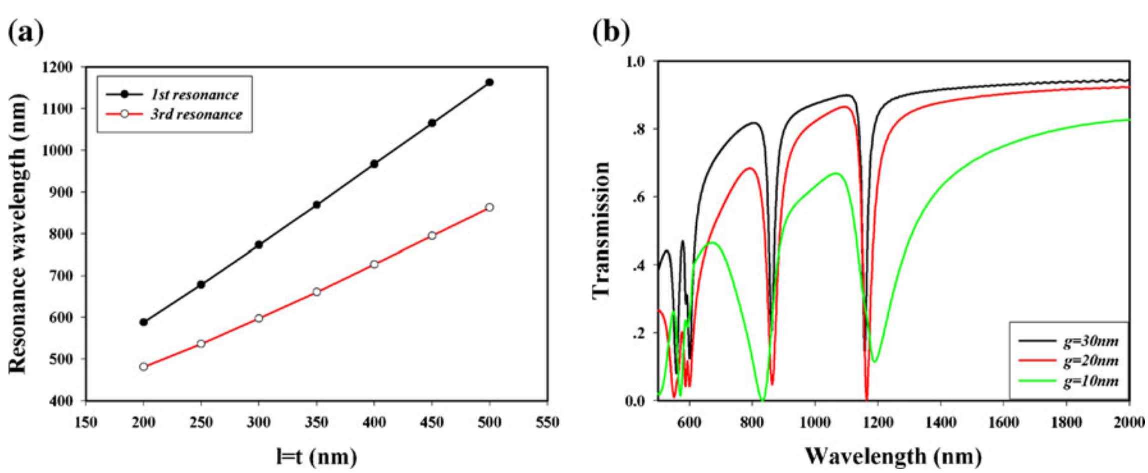

Fig. 6 **a** The resonance wavelength of the first and third mode of square cavity with different cavity sizes (g=30 nm). **b** The transmission spectra of square resonant cavity with different coupling gap sizes (l=t=500 nm)

cavity. It is clear that all the modes are WGM modes, which are formed by the interferences of the SPP waves at the Ag/air interface. The first mode (WG(1,1) mode) of the square resonant cavity (l=t=500 nm) is a TW mode, which splits into two SW modes when the resonant cavity changes from square to rectangle geometry. And the H_y fields of the two modes are distributed on the cavity wall along the x and z directions, respectively. Also, the H_y field distribution of the splitting second mode of the rectangle resonant cavity (l=480 nm, t=500 nm) is like that of the first mode of the rectangle resonant cavity (l=520, t=500 nm). The same trends are observed for the second mode and first mode of the rectangle resonant cavities with l=480 nm and l=520 nm, respectively. So, there is an intersection between the wavelengths of the first and second mode in Fig. 4 and the first mode with l<500 nm and the second mode with l>500 nm can be connected as a linear line. The third modes (WG (2,1) mode) of the square and rectangle resonant cavities are both SW modes, so the resonance wavelength only has a linear relation with the length l and increases with an increasing l just as a scaling effect of the cavity length. From Fig. 4, the fourth mode (WG (2,2) mode) has the same trend as the first mode, while the fourth mode is a SW mode. And when the geometry of the resonator changes from square to rectangle, the fourth mode of the square resonator is also degenerated into two SW modes (WG (2,2) mode), whose center H_y fields are coupled to the border of the cavity along x and z directions, respectively.

The above results show that there is an intersection between the resonance wavelengths of the first and second modes of the different rectangle resonant cavity sizes because of the mode degeneration. In order to show cavity size effects on the resonance wavelengths of the square resonant cavity, the resonance wavelengths of first and third modes according to different square cavity sizes are simulated and shown in Fig. 6a. It is obvious that the resonance wavelengths of the first and third modes of the square resonant cavity show linear relations with respect to the cavity sizes and increase with increasing cavity sizes, which is different from the rectangle resonant cavities. So, the filter wavelength can be linearly changed by altering the size of the square resonator. Then, the effects of the coupling gap size g on the transmission spectra are studied and the results are shown in Fig. 6b. The results show that the resonance bandwidth decreases by increasing the coupling gap size; in other words, the larger the coupling gap size, the larger the quality factor of the resonator can be realized. This is because by increasing the coupling gap size, coupling strength is reduced and more SPP energy can be stored in the resonant cavity. Also, it is clear that the resonance wavelengths are almost same except for a little shift due to the effective index perturbations of the coupling region.

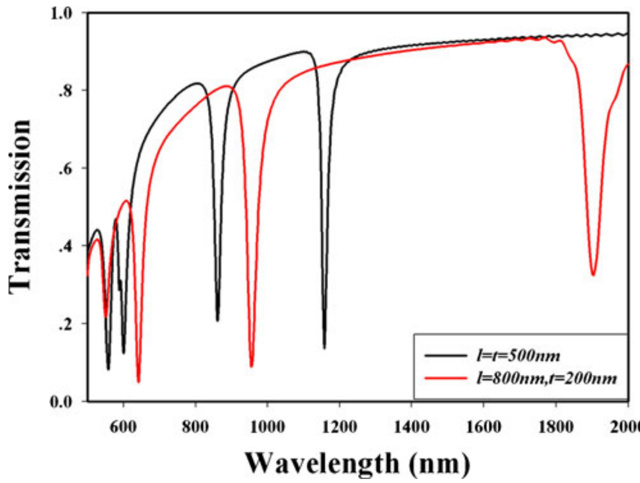

Fig. 7 Transmission spectra of rectangle resonant cavity (l=t=500 nm vs l=800 nm, t=200 nm)

All the modes in the above rectangle resonant cavities are the formed by the WGM because at the resonance wavelengths, the SPP fields at the silver/air interfaces in the cavity are independent and not coupled with each other very much, which can be clearly seen from the H_y field patterns. But when the width t or the length l is changed to a relative small value, the SPP fields at the opposite sides of the rectangle cavity are strongly coupled and the rectangle cavity can be treated as an MIM waveguide. Then, the Fabry–Perot (FP) modes can be formed in the rectangle resonance cavity [18], which are different from the WGM. In order to exclude the size effect of the resonant cavity, the perimeter of the rectangle resonant cavity (l=800 nm, t=200 nm) is kept the same as that of the square cavity (l=t=500 nm). The simulated transmission spectrum of the rectangle resonant cavity is compared with that of the square resonant cavity and is shown in Fig. 7. There

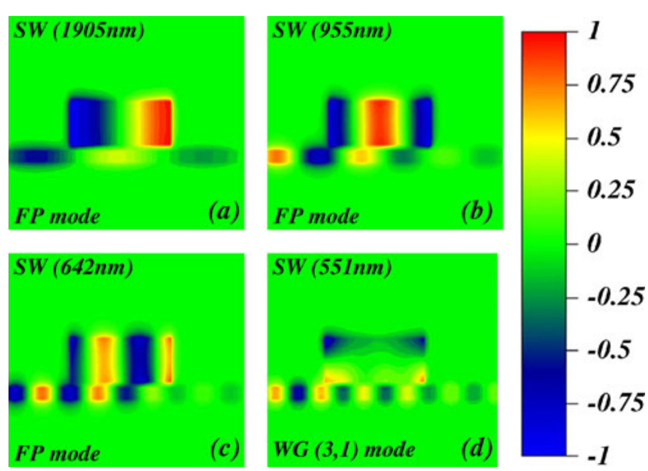

Fig. 8 *a–d* The H_y fields of the resonant modes of rectangle cavity (l=800 nm, t=200 nm)

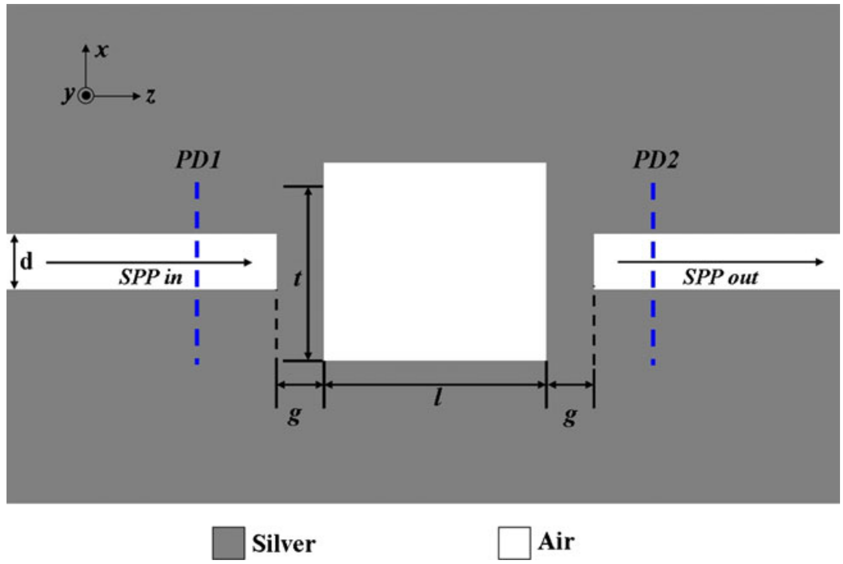

Fig. 9 The band-pass filter based on the direct-coupled rectangle SPP resonator

are also four resonance dips in the wavelength range but only the fourth mode resonance wavelength is consistent with that of the square cavity. Also, the H_y fields of the four resonant modes are shown in Fig. 8. From the H_y field distributions, we can conclude that the first three are the FP modes, while the last resonant mode with smallest resonance wavelength is the WGM because with this small wavelength, the SPP waves at the opposite silver/air interfaces are weekly coupled. So, in Fig. 7, only the resonance wavelength of the WGM mode of the rectangle cavity is accorded with that of the square cavity, while the other resonance wavelengths are different because of the different resonant mode types.

Mode Characteristics of the Band-pass Filter Based on Rectangle SPP Resonator

The band-stop-type SPP filter can be changed to a band-pass-type filter simply by changing from the side coupling to the direct coupling as shown in Fig. 9. The typical transmission spectra of the resonators with different square cavity sizes are shown in Fig. 10a. It can be concluded that there are fewer modes in the direct-coupled resonators than the side-coupled ones, which are caused by the different coupling conditions. Figure 10b shows that the resonance wavelength of the first mode of the square resonator follows the linear relation with the cavity size, which is the same as the side-coupled resonator. So, the SPP filter wavelength

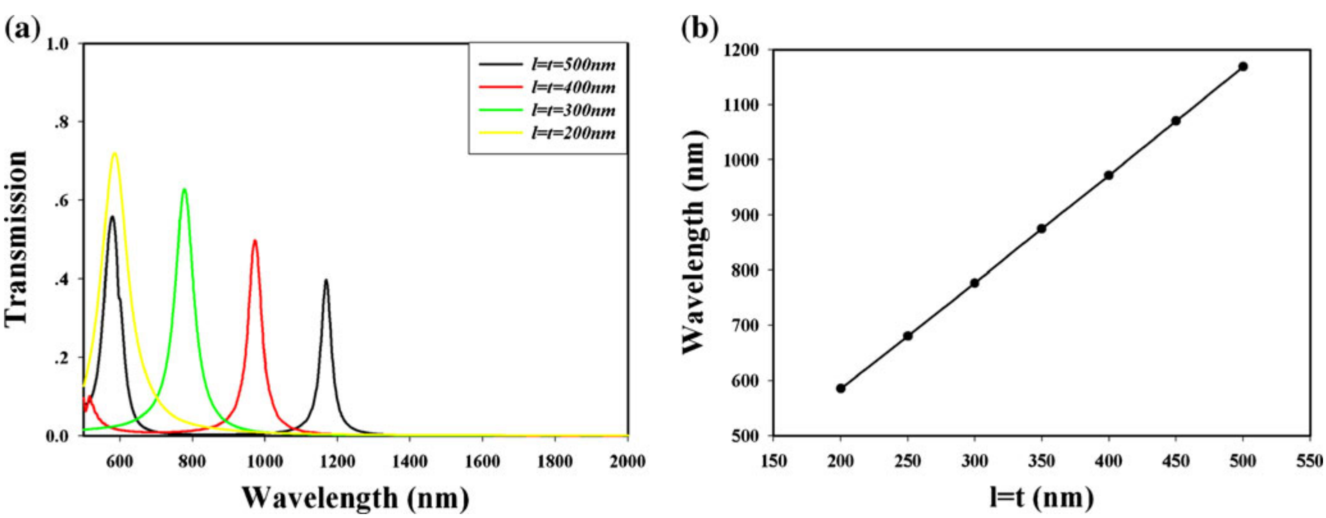

Fig. 10 **a** The transmission spectra of square resonator with different cavity size (g=20 nm). **b** The relation between the resonance wavelength of first mode and cavity size (g=20 nm)

can also be easily changed by altering the cavity size, which is very useful in the SPP integration applications. Also, the transmission spectra of the square resonator with different coupling gap sizes are shown in Fig. 11. It is obvious that the bandwidth of the resonance increases with a decreasing gap size just as the side-coupled resonator. The transmission peak value is increased with a decreasing gap size. So, there is a contradiction between the transmission and the quality factor. Also, there are small resonance peak wavelength shifts for different coupling gap sizes due to the small perturbation of the SPP effective index in the coupling region.

Finally, the resonance wavelengths of the different resonant modes of the direct-coupled rectangle cavities are shown in Fig. 12. The results show that the resonance wavelength of the first mode increases linearly with an increasing length l, while the resonance wavelengths of the second and third modes are intersected when the cavity is square in shape (l=t=500 nm). This phenomenon is like that of the first and second modes of side-coupled resonators in Fig. 4. Here, the second mode of the square resonator is degenerated to two modes (second and third) in the rectangle resonator. The corresponding H_y fields are also shown in Fig. 13. Both the SW and the TW modes are supported by the direct-coupled resonator, which just is like the side-coupled resonators. Besides, the hybrid modes of the SW and the TW modes also exist, which are not supported by the side-coupled resonators. These hybrid modes maybe caused by the perturbations of the coupling MIM waveguides.

According to the above results, the rectangle SPP resonators are highly geometric-dependent and can support both the traveling-wave modes and standing-wave modes, which are different from that of the classical

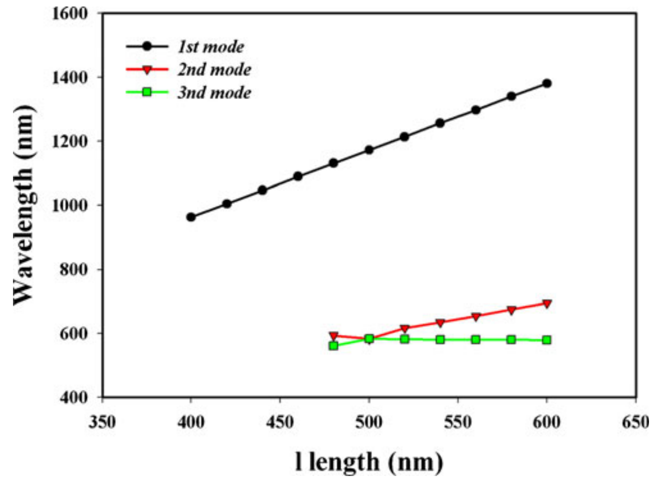

Fig. 12 Resonance wavelengths of rectangle resonator with different l (t=500 nm, g=10 nm)

Fabry–Perot resonator, where only the standing-wave modes can be realized. For the side-coupled band-stop SPP rectangle filter, the traveling-wave mode can only be realized by the WG mode with the square-shaped SPP resonator, while the standing-wave mode can be realized by both the WG mode and the FP mode. And the traveling-wave mode is splitted into two standing-wave modes by transforming the cavity shape from square to rectangle. Also, for the direct-coupled band-pass SPP rectangle filter, both the SW and TW modes are supported, like the side-coupled resonators. Besides, the hybrid modes of SW and TW modes also exist, which are not supported by the side-coupled resonators. By comparing to the classical dielectric waveguide approach, the mode size of SPP waveguide can be greatly reduced because of its strong bonding capability at the dielectric/metal interface, which can greatly reduce the component size. Also, with this very strong bonding capability, the bending loss at the 90° corner in the rectangle cavity is greatly reduced and can be neglected, while for the class dielectric waveguide, very high bending loss will be introduced, which is an inherent defect of the dielectric waveguide.

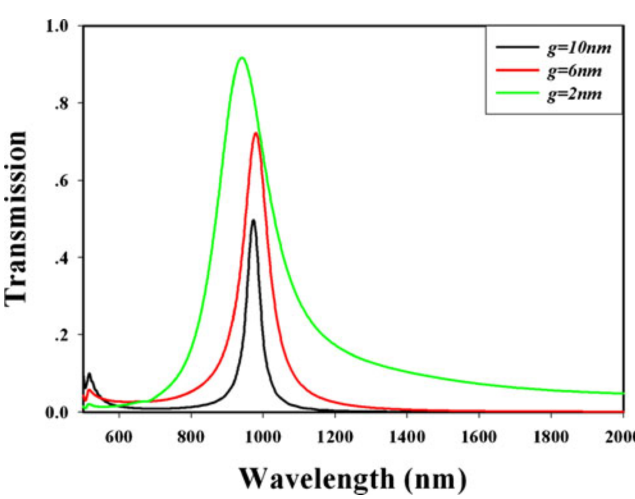

Fig. 11 The transmission spectra of the square resonant cavity with different coupling gap sizes (l=t=400 nm)

The rectangle SPP resonator can be fabricated by the focused ion beam method [27] on a silver film. In order to analyze the effect of the fabrication uncertainties on the SPP square resonator (l=t) which has the traveling-wave mode, the variation of the side length l relative to the side length t is taken into account. Figure 14 shows the transmission spectrum of the side-coupled rectangle SPP resonator (l=495 nm, t=500 nm), where the difference of the two side lengths is 5 nm. It is obvious that the first and the second standing-wave modes shown in Fig. 3 are merged into one traveling mode, which is the characteristic of the square resonator. So, in order to realize the traveling-wave mode of the square resonator,

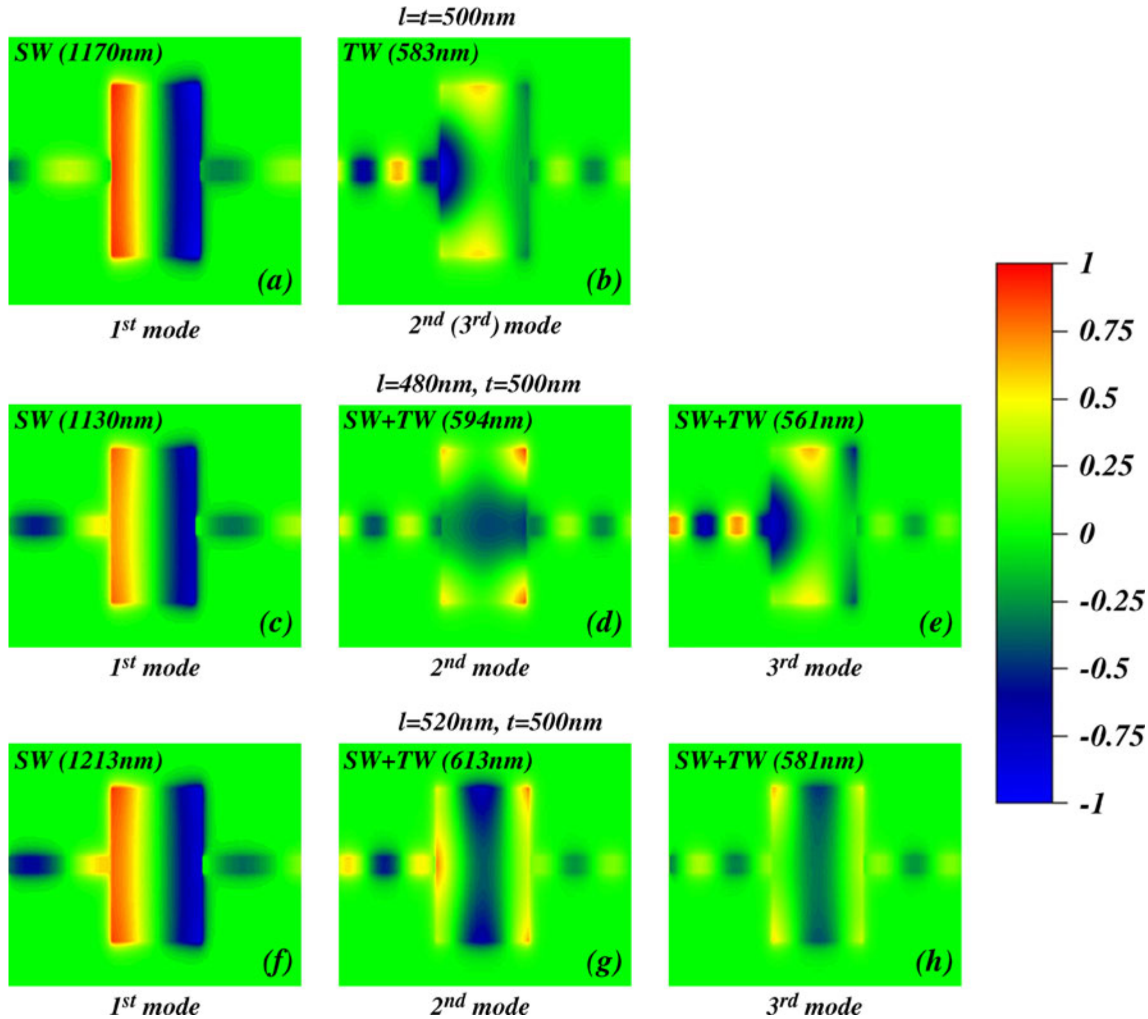

Fig. 13 *a–h* The H_y fields of the resonant modes with different geometries

the side length difference of the resonator should not be larger than ±5 nm.

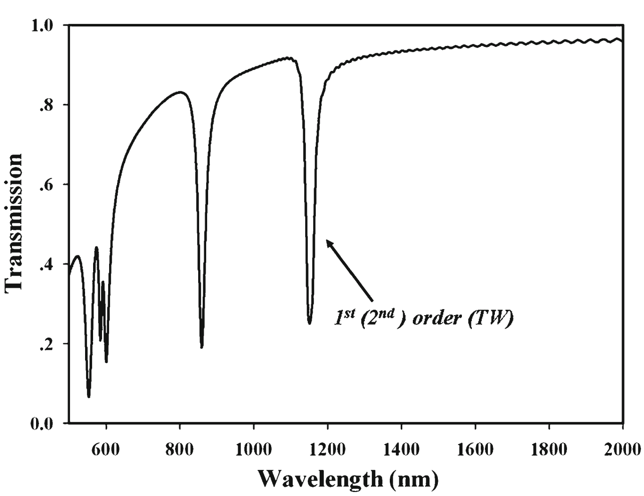

Fig. 14 The transmission spectrum of rectangle cavity (l=495 nm, t=500 nm, g=30 nm)

Conclusion

In this article, the characteristics of the resonant modes in the side-coupled (band-stop filter) and direct-coupled (band-pass filter) SPP rectangle cavities are studied and analyzed in detail. The whispering gallery mode and the Fabry–Perot mode can be supported by the rectangle SPP resonator. Furthermore, both traveling-wave mode and standing-wave mode can be realized by the WGM, while only standing-wave mode can be introduced by the FP mode. For the side-coupled resonator, the traveling-wave mode can be degenerated into two standing-wave modes by changing the resonator cavity from square to rectangle geometry, while for the direct-coupled resonator, the traveling-wave mode degenerates into two hybrid modes by changing the resonator cavity from square to rectangle geometry. And for the resonators with square cavities, the resonance wavelengths change linearly according to the cavity sizes.

Acknowledgments This work was supported by the National Science Foundation of China under grant no. 60907025 and Science Foundation of Southeast University under grant no. KJ2009358.

References

1. Barnes WL, Dereux A, Ebbesen TW (2003) Surface plasmon subwavelength optics. Nature 124:824–830
2. Ozbay E (2006) Plasmonics: merging photonics and electronics at nanoscale dimensions. Science 311:189–193
3. Berini P (2009) Long-range surface plasmon polaritons. Adv Opt Photon 1(484):588
4. Kim JT, Jung Jin Ju, Park S, Kim Min-su, Park SK, Lee M-H (2008) Chip-to-chip optical interconnect using gold long-range surface plasmon polariton waveguides. Opt Exp 16:13133–13138
5. Bozhevolnyi SI, Volkov VS, Devaux E, Laluet J-Y, Ebbesen TW (2006) Channel plasmon subwavelength waveguide components including interferometers and ring resonators. Nature 440:508–511
6. Bozhevolnyi SI, Volkov VS, Devaux E, Ebbesen TW (2005) Channel plasmon-polariton guiding by subwavelength metal grooves. Phys Rev Lett 95:046802
7. Han Z, Van V, Herman WN, Ho PT (2009) Aperture-coupled MIM plasmonic ring resonators with sub-diffraction modal volumes. Opt Exp 17:12678–12684
8. Xiao S, Liu L, Qiu M (2006) Resonator channel drop filters in a plasmon-polaritons metal. Opt Exp 14:2932–2937
9. Wang TB, Wen XW, Yin CP, Wang He Zhou (2009) The transmission characteristics of surface plasmon polaritons in ring resonator. Opt Exp 17:24096–24101
10. Han Z (2010) Ultracompact plasmonic racetrack resonators in metal-insulator-metal waveguides. Photonics Nanostruc 8:172–176
11. Hosseini A, Massoud Y (2007) Nanoscale surface plasmon based resonator using rectangle geometry. Appl Phys Lett 90:181102
12. Liu J, Fang G, Zhao H, Zhang Y, Liu S (2010) Plasmon flow control at gap waveguide junctions using square ring resonators. J Phys D 43:055103
13. Yun B, Guohua Hu, Cui Y (2010) Theoretical analysis of a nanoscale plasmonic filter based on a rectanglar metal-insulator-metal waveguide. J Phys D 43:385102
14. Matsuzaki Y, Okamoto T, Haraguchi M, Fukui M, Nakagaki M (2008) Characteristics of gap plasmon waveguide with stub structures. Opt Exp 16:16314–16325
15. Tao J, Huang XuGuang, Liu SongHao (2010) Optical characteristics of surface plasmon nanonotch structure. J Opt Soc Am B 27:1430–1434
16. Liu J, Fang G, Zhao H, Zhang Y, Liu S (2009) Surface plasmon reflector based on serial stub structure. Opt Exp 17:20134–20139
17. Lin XS, Huang XG (2008) Tooth-shaped plasmonic waveguide filters with nanometeric size. Opt Lett 33:2874–2876
18. Yun B, Guohua Hu, Cui Y (2011) A nanometric plasmonic waveguide filter based on Fabry-Perot resonator. Opt Comm 284:485–489
19. Qin Zhang Xu, Huang G, Lin XS, Tao J, Jin XP (2009) A subwavelength coupler-type MIM optical filter. Opt Exp 17:7549–7554
20. Lee PH, Lan YC (2010) Plasmonic waveguide filters based on tunneling and cavity effects. Plasmonics 5:419–422
21. Hua Lu, Liu X, Gong Y, Wang L, Mao D (2011) Multi-channel plasmonic waveguide filters with disk-shaped nanocavities. Opt Comm 284:2613–2616
22. Wang G, Hua Lu, Liu X, Mao D, Duan L (2011) Tunable multi-channel wavelength demultiplexer based on MIM plasmonic nanodisk resonators at telecommunication regime. Opt Exp 19:3513–3518
23. Noual A, Pennec Y, Akjouj A, Djafari Rouhani B, Dobrzynski L (2009) Nanoscale plasmon waveguide including cavity resonator. J Phys Condens Matter 21:375301
24. Yu Z, Veronis G, Fan S, Brongersma ML (2008) Gain-induced switching in metal-dielectric-metal plasmonic waveguides. Appl Phys Lett 92:041117
25. Tao J, Huang XG, Zhu JH (2010) A wavelength demultiplexing structure based on metal-dielectric-metal plasmonic nano-capillary resonators. Opt Exp 18:11111–11116
26. Rakic AD, Djurisic AB, Elazar JM, Majewski ML (1998) Optical properties of metallic films for vertical cavity optoelectronic devices. App Opt 37:5271–5283
27. Ernst JR, Vesseur FJ, de Abajo G, Polman A (2009) Modal decomposition of surface-plasmon whispering gallery resonators. Nano Lett 9:3147–3150